Structural Chemistry (2019) 30:955–963
https://doi.org/10.1007/s11224-018-1239-5

ORIGINAL RESEARCH

Electronic structure and stability of anionic $AuGe_n$ ($n = 1–20$) clusters and assemblies: a density functional modeling

Debashis Bandyopadhyay [1]

Received: 4 October 2018 / Accepted: 15 November 2018 / Published online: 10 December 2018

Abstract

In the present study electronic structure and stabilities of cationic gold-doped germanium clusters, $AuGe_n$ ($n = 1$ to 20), and their assemblies have been investigated by density functional theory (DFT) modeling. Computational results show a good relationship between the thermodynamic parameters, average binding energy, embedding energy, fragmentation energy, etc., with the percentage hybridization between different Ge 4*s*, Ge 4*p*, and Au *5d* atomic orbitals, which plays a dominating role in the stabilization of anionic $AuGe_7$, $AuGe_{10}$, $Au(Ge_7)_2$, $Au(Ge_9)_2$, and $Au(Ge_{10})_2$ clusters. Other thermodynamic and chemical parameters are also found consistent with the observed thermodynamic stabilities of the nanoclusters. In smaller size range ($n < 11$), Au atom always absorbs on the surface or vertex of pure Ge cluster. From $n = 11$, endohedral doping starts. In the assembled clusters, Au atom play the role as a bridging atom in $Au(Ge_7)_2$, $Au(Ge_9)_2$, and $Au(Ge_{10})_2$ clusters. Stability of the $AuGe_7$, $AuGe_{10}$, $Au(Ge_7)_2$, $Au(Ge_9)_2$, and $Au(Ge_{10})_2$ are explained using magic number in shell-filled model and mixed (π-σ) aromatic rule. As per the symmetry and structure of $AuGe_{12}$ cluster, it is comparable to a nido-cluster, and hence, its stability is explained using Wade-Mingos rule. Calculated VDE, ADE, HOMO-LUMO gap, and VIP have very close agreement with the experimental results. IR and Raman frequencies show that the vibration nature of the clusters could produce electromagnetic radiation in the far infrared region which is useful for medical applications.

Keywords Density functional theory · Cluster and cluster assembly · Electronic structure · ADE and VDE · IR and Raman · DOS

Introduction

The group IV-A clusters, especially silicon and germanium encapsulated by transition metals, continue to attract much attention due to their potential as assembled nanomaterials in the field of microelectronic and nanoelectronic industries. Recently, the main focus in this filed got shifted to explore the stability and electronic structures of these nanoclusters where the role of valance electrons in hybridization is supposed to be crucial [1–13]. Pure silicon and germanium clusters are usually unstable due to presence of unsaturated bonds over the surfaces of the clusters. Encapsulation of transition metals atom(s) with the pure semiconductor clusters absorbs the dangling bonds and enhances the stability of the clusters. Among the group 14 elements in periodic table, Ge always is an ideal replacement of Si because of its higher electron and hole mobility [14,15]. Therefore, Ge-based hybrid semiconductors need to explore for new materials with potential applications in electronic industries.

In recent time, a number theoretical and experimental studies on the electronic structures, thermodynamic and chemical properties, stabilities, etc., of transition metal (TM)-doped germanium clusters are reported [16–26]. These studies show that the doping of TM atoms not only improves the stabilization of pure germanium cages but also modifies the property of these nanoclusters in a wide range by adapting HOMO-LUMO gap, spin states, and the charge transfer nature between the pure Ge cages and the TM metal atoms. It is also possible to model a cluster-assembled materials with specific electronic and magnetic properties by modifying the pure germanium cluster as a unit of cluster-assembled materials after TM metal doping. To understand the stability of these nanoclusters, the electronic structures of the nanoclusters are explained on the basis of the electron-counting rule, shell-filled model, three-dimensional aromatic properties of the cluster, electron localization

Electronic supplementary material The online version of this article (https://doi.org/10.1007/s11224-018-1239-5) contains supplementary material, which is available to authorized users.

✉ Debashis Bandyopadhyay
debashis.bandy@gmail.com

[1] Department of Physics, Birla Institute of Technology and Science, Pilani, Rajasthan 333031, India

function, etc. However, enhanced stability of some of the clusters obtained experimentally and theoretically sometimes cannot be explained using these existing rules [27–33]. This fact essentially makes existing rules somewhat unclear. However, in the demand of stability, Reveles and Khanna [34] raised the presence of free electron gas formed by the valence electrons inside the TM-Si cluster cages and explained the stability of different magnetic nanoclusters on the basis of existing electron-counting rules. It is important citing here that in phenomenological shell model, one-electron levels in spherically confined free-electron gas and the clusters having 2, 8, 18, 20, 34, 40 58, 68, etc., number of valance electrons fulfill the shell-filling numbers and attain enhanced stability. As an example, the higher abundance of neutral $TiSi_{16}$, cationic VSi_{16}, and anionic $ScSi_{16}$ clusters in the experimental study of Koyasu et al. [35] follow the shell-filled model with 68 valance electron structure.

With the current standing of this field, the present study set to carry out a systematic investigation on $AuGe_n$ ($n = 1$–20) clusters in anionic state with an aim to explore its potential as a designer material. Gold has large electronegativity and high electron affinity. One can explore it to achieve a cluster-assembled material with potential applications. Furthermore, due to the high thermoelectric power and hot electron effect, gold-doped germanium clusters are useful in fabrication of thermopiles [36], cryogenic phonon sensors [37], etc. A number of theoretical and experimental investigation on gold-doped germanium clusters have been reported before [38–44]. The present study is focused on to explain the stability of the clusters from the electronic structure of the clusters and their assemblies within the size range of $n = 1$–20.

Computation

In the present study, all structural optimization of the predicted geometries of the $AuGe_n$ clusters are performed within the framework of generalized gradient approximation (GGA) with the PBE exchange-correlation functional [45,46] under density functional theory (DFT) as executed in the Gaussian '09 package program [47]. Standard Gaussian-type basis sets cc-pvtz for Ge atom and the scalar relativistic effective core potential Stuttgart/Dresden (SDD) basis set [48] (also available in Gaussian '09 package) for the Au atom are used to express the molecular orbitals (MOs) of all atoms as linear combinations of atom-centered basis functions. All geometry optimizations are performed with no symmetry constraints. During optimization, it is always possible that a cluster with particular guess geometry can get trapped in a local minimum of the potential energy surface. To avoid this, the global search method (structure prediction) by using USPEX [49] is employed at the beginning of the geometry selection of the bigger sized ($n > 5$) clusters. The predicted geometries are then optimized using VASP [50–54] to get global ground state geometry in each size (Electronic Supplementary Information). In the next stage, the globally optimized ground state isomers are again re-optimized using Gaussian '09 as mentioned above to get more accurate information about the geometry. Self-consistent field processes during geometry optimization are carried out with a convergence criterion of 10^{-6} Hartree on the energy and electron density. The vertical detachment energies (VDEs) are calculated as the energy differences between the neutral (in doublet-spin state) and anionic clusters (in singlet-spin state), both at the optimized geometries of anionic classes. The adiabatic detachment energies (ADEs) were calculated as the energy differences between the neutral molecules and anions after relaxing the anionic cluster geometry (in singlet-spin state) in neutral state (in doublet-spin state). The ground state energies of the stable clusters in each size are corrected by including the zero-point energy (ZPE) of the clusters.

Results and discussions

Energetics and stability

Calculated optimized structures obtained by using USPEX and VASP are more or less similar to the previous reports [44, 55–57] for the sizes less than $n = 14$. Selected low-lying optimized isomers in each size are shown in Electronic Supplementary Information (ESI Fig. 1). To monitor the relative stabilities of anionic $AuGe_n$ clusters, different thermodynamic parameters, such as the average binding energy (BE), fragmentation energy (FE or $\Delta_{n,n-1}$), and second-order change in energy (relative stability parameter or Δ_2), are studied. Based on the thermodynamic parameters, $AuGe_7$, $AuGe_{10}$, and $AuGe_{12}$ are found most stable species. Further, bigger-sized stable clusters are found as cluster assemblies. These assemblies are the combination of $AuGe_7$(cationic) + Ge_7(neutral cage), $AuGe_9$(cationic) + Ge_9 (neutral cage), and $AuGe_{10}$(cationic) + Ge_{10} (neutral cage). These clusters can be better understood by taking Au as breeding atom between Ge_n cages. So, these stable cationic clusters can also be represented as Ge_7-Au-Ge_7 (i.e., $Au(Ge_7)_2$), Ge_9-Au-Ge_9 (i.e., $Au(Ge_9)_2$), and Ge_{10}-Au-Ge_{10} (i.e., $Au(Ge_{10})_2$). The average binding energy per atom of these clusters in general is defined as $BE = (nE_{Ge} + E_{Au} - E_{AuGe_n})/(n+1)$. It calculates the energy gained during the formation of cluster from individual atoms, where n is the number of Ge atoms in the cluster. The variation of binding energies is shown in Fig. 1. With reference to Fig. 1, $n = 5$, 7, 10, 12, and the clusters assemblies with $n = 14$, 18, and 20 are identifies as the stable clusters. At the lower size, the variation in BE with the cluster size is relatively higher than the bigger sizes. This is the indication of thermodynamic

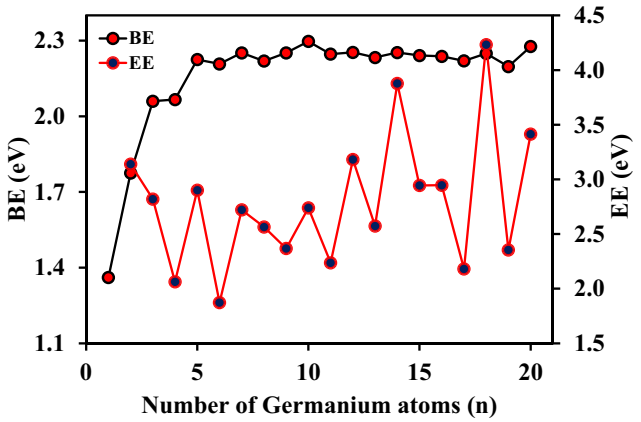

Fig. 1 Variation of average BE and EE of anionic $AuGe_n$ ($n = 1$–20) ground state clusters with the cluster size (n)

instability of the smaller-sized clusters. In the binding energy variation, there are a number of local maxima, at $n = 7$, 10, 12, 14, 18, and 20. These local maxima are indicating thermodynamic stability of the clusters. In this context, it is important to mention that in general embedding energy (EE) of a cluster series follow the same trend as BE. Embedding energy can be defines as $EE = E_{AuGe_n} - E_{Ge_n} - E_{Au}$. So, positive value of the embedding energy always indicates the higher stability, and this can be seen in the present study. Variation of embedding energy that is presented in Fig. 1 supports the variation of BE. It shows local maxima at $n = 7$, 10, 12, 14, 18, and 20. In the previous experimental study on the same system followed by a theoretical calculation by Lu et al. [44], endohedral anionic $AuGe_{12}$ (I_h symmetry) with icosahedral structure is identified as the most stable isomer, which has been justified by shell model which will be discuss in the later section. In the present study, we have also identified the same structure as local maxima. To further check the stability of the clusters during the growth process and to answer a related but slightly different question during the growth process by adding one by one Ge atom to the Ge-Au dimer, the fragmentation energy and the second-order difference in energy (Δ_2) are calculated following the relations given as

$$\Delta_{n,n-1} = -E_{AuGe_{n-1}} + E_{Ge} - E_{AuGe_n} \text{ and } \Delta_2 = -E_{AuGe_n} + E_{AuGe_{n-1}} - 2E_{AuGe_n}$$

According to the definition, higher positive values of these parameters indicate higher stability of the clusters compared to its immediate smaller and next bigger clusters during growth process. Variations of FE and relative stability with the cluster size are shown in Fig. 2. These parameters also supported the stability results of BE and EE parameters. Variation of these four thermodynamic parameters always show the enhanced stability of anionic $AuGe_7$, $AuGe_{10}$, $AuGe_{12}$, $Au(Ge_7)_2$, $Au(Ge_9)_2$, and $Au(Ge_{10})_2$ clusters. As mentioned earlier, enhanced stability of the clusters can be efficiently explained in terms of electronic shell models developed for metal clusters. It has been shown for metal clusters that whenever a new shell starts getting occupied for the first time, the vertical ionization potential (VIP) and vertical (and adiabatic) detachment energy, VDE (and ADE), drop sharply. In the present report, variation of calculated VDE and ADE along with the experimentally obtained results [44] are shown in Fig. 3. The variations of calculated VDE and ADE are more or less similar to the experimentally obtained vertical detachment energies (VDE and ADE) by Lu et al. [44] and show that sharp peaks at $n = 7$, 10, 12, 14, 18, and 20 indicate the stability of these clusters. Similar picture is found in the variation of vertical ionization potential (VIP) and HOMO-LUMO gap of these clusters (Fig. 4). Kinetic stability of the clusters can be obtained from the presence of local maxima of the HOMO-LUMO gap (ΔE) variation of the clusters during growth process. With reference to Fig. 4, local maxima in HOMO-LUMO gap support the higher chemical stability of the clusters with $n = 7$, 10, 12, 14, 18, and 20. All the stable clusters have large HOMO-LUMO gaps as 1.64 eV, 1.723 eV, 1.90 eV, 1.12 eV, 1.19 eV, and 1.68 eV for $AuGe_7$, $AuGe_{10}$, $AuGe_{12}$, $Au(Ge_7)_2$, $Au(Ge_9)_2$, and $Au(Ge_{10})_2$, respectively. Overall, there is a local oscillation in HOMO-LUMO gap. Variation of VIP is perhaps the most important parameter to examine the stability of the clusters. The nature of variation of VIP and HOMO-LUMO gaps is similar with the local minima at the same cluster sizes. Overall VIP values decrease continuously with the increase of the cluster size. Therefore, both thermodynamic and chemical parameters support the enhance stability of $n = 7$, 10, 12, 14, 18, and 20 clusters. To understand the charge exchange between the germanium cage and the embedded Au atom during hybridization with the germanium cluster, variation of charge on the Au atom and the average charge per Ge atom in the ground state $AuGe_n$ clusters as a function of the size of the cluster is calculated using Mulliken charge population analysis and is presented in Fig. 5. It is well known that after doping of transition metal atom in Ge clusters, TM atom behaves as electron donner to the Ge_n cage and enhances the stability of the clusters. In the present work, it is found that for $n = 12$, there is a drastic change in the charge value. This is because of highly symmetric nature of the ground state anionic $AuGe_{12}$ cluster that gives enhanced stability to this cluster. The theoretical stability of anionic $AuGe_{12}$ has been explained by Wade-Mingos [58–60] rule and shell-filled structure obtained from electronic shell perspective.

Stability and electronic shell model

From the results we have obtained from the energetics of the clusters, it is clear that not a single, but a number of clusters can be accepted as theoretically stable clusters in single anionic state. Since most of these stable clusters are holding shell-filled number or are close to shell-filled number, therefore, in

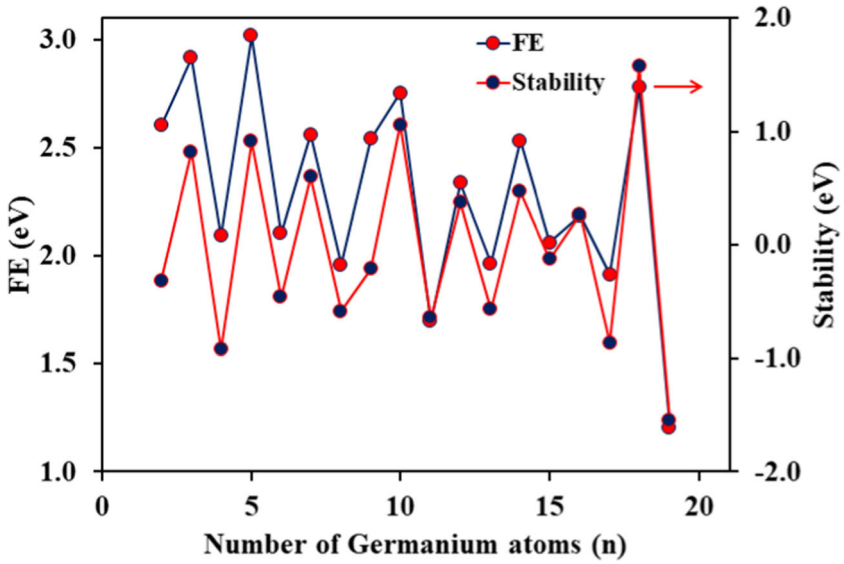

Fig. 2 Variation of FE and stability parameter of anionic $AuGe_n$ ($n = 1–20$) ground state clusters with the cluster size (n)

this section their stability will be explained from the electron shell perspective. As per the recent reports [61–63] on highly stable metal-doped Si, Ge, Sn, and Pb cage clusters, the main cause of their stability is identified as due to the strong hybridization between the transition metal atom with the host cages when the electron energy states of the single electron orbital of the cluster follow the shell model sequence. Within the shell model, the successive occupation of a level, giving a magic number, leads to a stabilized cluster. According to the phenomenological shell model, the valance electrons in a cluster are usually delocalized over the surface of the whole cluster, whereas the nuclei and core electrons can be replaced by their effective mean-field potential. Therefore, theoretically calculated molecular orbitals S, P, D, F, G, etc., of the clusters are expected to have the similar shape to those of the *s*, *p*, *d*, etc., atomic orbitals. The sequence of the electronic shells depends on the shape of the restricting potential used in the calculation. In general, for a spherical cluster with a square well potential, the orbital sequence is $1S^2$, $1P^6$, $1D$,[10] $2S^2$, $1F^{14}$, $2P^6$, $2D$,[10] $1G^{18}$, and $1H^{22}$ corresponding to close shell structure with 2, 8, 18, 20, 34, 40, 58, 68, 90, … number of electrons.

The clusters with enhanced stability obtained from the energetics analysis with $n = 7$, 10, 12, 14, 18, and 20 are having 40, 52, 60, 68, 84, and 92 number of valance electrons, which are the shell-filled number or close to the shell-filling numbers. The first member of these stable clusters is anionic $AuGe_7$ holding 40 valence electrons which is a shell-filled number. The single-electron orbitals are shown in ESI Fig. 2. Out of these 40 electrons, six 2D electrons are assigned in non-bonding (NB) orbitals. Therefore, the revised orbital sequence becomes $1S^2$; $1P^6$; $1D^6$; $2D^2$(NB); $2D^4$; $2D^4$ (NB); $2S^2$; $1D^4$; $1F^4$; $2P^6$. Though, all orbitals are not total filled, but the top most $2P^6$ orbitals is completely field and fulfilling the shell-filled number 34 that gives enhance stability to this cluster. Distributions of

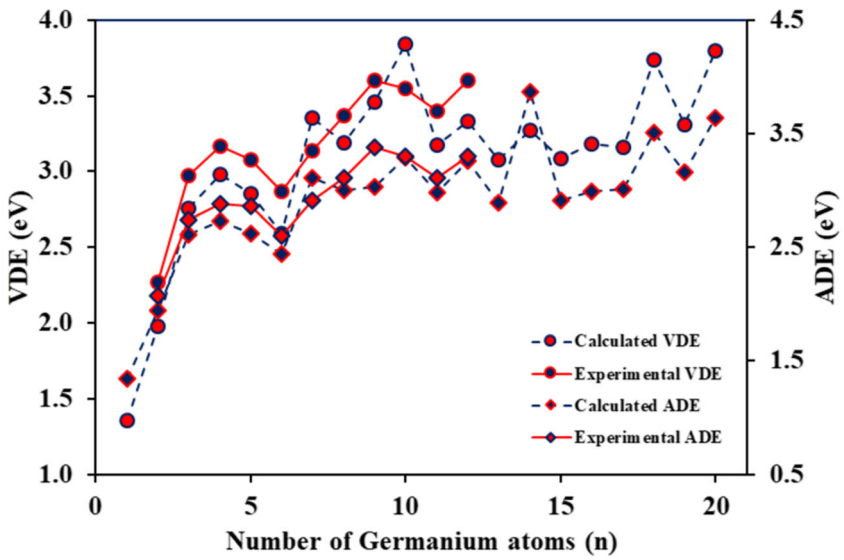

Fig. 3 Variation of reported and calculated VDE and ADE of anionic $AuGe_n$ ($n = 1–20$) ground state clusters with the cluster size (n)

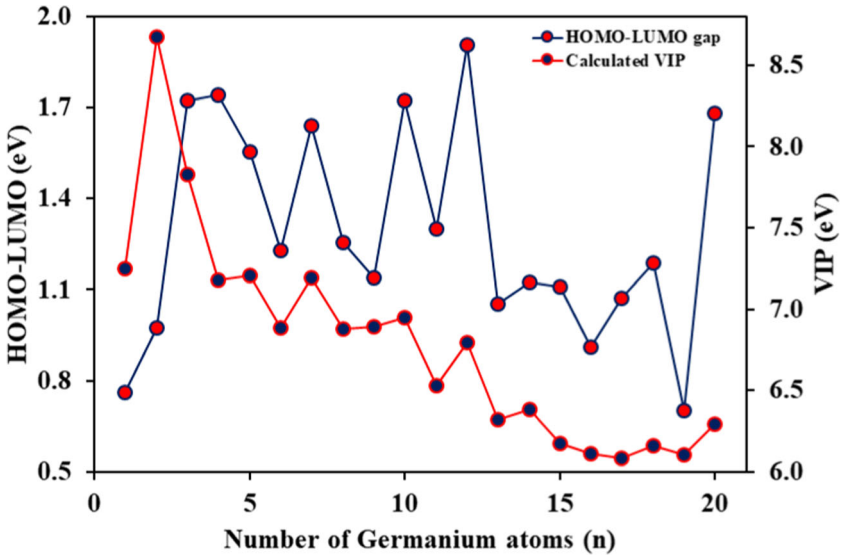

Fig. 4 Variation of HOMO-LUMO gap and VIP of anionic and neutral $AuGe_n$ ($n = 1–20$) ground state clusters, respectively, with the cluster size (n)

these electrons' energy levels are shown in density of state distribution (DOS) in (ESI Fig. 3), and degeneracy in energy levels are shown in (ESI Fig. 4). To understand DOS clearly, the degenerate energy levels are presented. In each energy level, group contribution of Ge atoms and Au atom is shown. In the lower energy levels, dominating contribution comes from Gr group, whereas in the higher orbitals, Au contribution is more compared to the lower energy levels. It is to be noted that dominating contributions in the assigned non-bonding orbitals are from Au. So, there is clear significance between the similarity of orbitals, DOS, and energy levels.

The ground state of pure Ge_{10} is bi-capped antisymmetric square prismatic structure with D_{4d} symmetry. It has total 40 valance electrons (which is a shell-filled number) in the sequence: $1S^2$ $1P^6$ $1D^{10}$ $1F^4$ $2S^2$ $1F^{12}$ $2P^6$ (ESI Fig. 2). Therefore, all 1S, 1P, 1D, 2S, 2P, and 1F levels are completely filled. Hence, the structure has enhanced stability. Addition of Au at endohedral position does not improve the stability, and finally, it takes a position which is connected to a vertex Ge atom appearing as a global ground state at this size. In anionic $AuGe_{10}$, total 52 electrons are distributed in the sequence: $1S^2$; $1P^6$; $1D^{10}$; $1F^2$; $2D^{10}$; $2S^2$; $1F^{10}$; $2P^2$; $1F^2$; $1F^{*2}$; $2P^4$ with a number of P, D, and F double-degenerated levels as shown in (ESI Fig. 4). Corresponding total density of states (DOS) and with the position of these energy levels are shown in (ESI Fig. 3). From the (ESI Fig. 4), degenerate orbitals and corresponding strength in DOS can be seen. The first peak in DOS in the lower energy side is purely due to $1S^2$ contribution from Ge group of atoms. Next, DOS is the overlap between $1P^2$ and degenerated $1P^4$ orbitals. Here also, Au contribution is negligible. All $1D^{10}$ orbital contribution grouped together in DOS. Here also, Ge cage contribution is dominating. Clearly, the first $1F^2$ orbital is due to overlap between the Ge cage and Au atom. Therefore, in DOS, both of these contributions are comparable. In the eighth

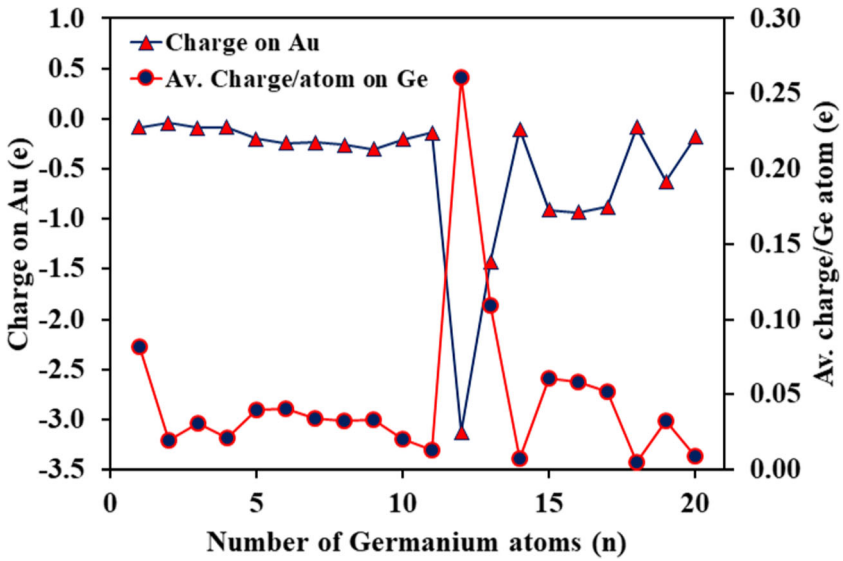

Fig. 5 Variation of charge on Au and average charge/Ge atom in $AuGe_n$ ($n = 1–20$) ground state clusters with the cluster size (n)

and ninth peaks of DOS, though the dominating contribution is from Au –2D orbital, but considerable amount of cage contributions can be seen clearly at the beginning. The first three Au – 2D orbitals are very close (ESI Fig. 4). Among these three, the lowest-energy one is a mixture of NB Au $2D_Z^2$ and cage $1S^2$ orbitals. Therefore, in DOS, a considerable amount of cage contribution can be found. Next two degenerated levels are well separated that followed by $2S^2$ orbital. Following the group contribution in DOS, the higher peaks in DOS are mainly due to the cage contribution. Above $2S^2$ orbital, two degenerated F orbitals are $F\sigma_{x(x^2-3y^2)}$ and $F\sigma_{y(3x^2-y^2)}$. In the sequence, the next significant orbital is HOMO-2, which is due to formation of antibonding between Au-d and Ge_{10} F_z orbitals and assigned as $1F_z^*$. Therefore, both 1F and 2P orbitals are completely filled. Excluding $2D^{10}$ non-bonding and $1F^{*2}$ antibonding electrons, total 40 electrons are fulfilling the shell-filled number. Hence, it gives higher stability to this cluster. Here, LUMO is $1G^2$ energy levels. In a recent theoretical investigation [43], the orbital sequence of neutral $CuGe_{10}$ (D_{4d}) is found as $1S^2$, $1P^6$, $1D^{10}$, $2D^{10}$, $2S^2$, $1F^{14}$, $1P^6$, $1G^1$. Further, following the work of Truong and Nguyen [41] and Hirsch et al. [64], to understand the stability of anionic $AuGe_{10}$ cluster, effect of spherical aromaticity on it is applied, where π-electrons are approximately considered as spherical electron gas that spread over the spherical (approximate) surface of the cluster. As per their report, the stability in cationic $CuGe_{10}$ cluster is due to σ-π mixed automaticity. In the present case, in the ground state of anionic $AuGe_{10}$ cluster, $2D^{10}$ molecular orbitals are non-bonding orbitals. In the remaining 42 electrons, $1S^2(\sigma)$, $1P^6(\sigma)$, $1D^{10}(\sigma)$, $1F^2(\sigma)$, $1F^4(\sigma)$, $1F^4(\sigma)$, and $1F^4(\sigma)$, i.e., 32 σ-electrons, and $2S^2(\pi)$, $2P^2(\pi)$, and $2P^4(\pi)$, i.e., 8 π-electrons. As per the mixed (π-σ) aromatic rule discussed by Hirsch et al. [64], both 32 σ-electrons and 8 π-electrons follow $2(n+1)^2$ counting rule for $n = 3$ and 1, respectively. Therefore, sigma electrons and pi-aromaticity enhance the stability of the cluster.

In general, the icosahedron $TMGe_{12}$ structures with D_{5h} symmetry give enhanced stability mainly because of its structural symmetry. In the present case, the cationic $AuGe_{12}$ icosahedron structure with D_{5h} symmetry also shows enhance stability compared to the other clusters in the same size. As we have obtained from the study of energetics, it shows local maxima in BE, EE, VDE, VEA, VIP, and HOMO-LUMO gap. It has total 60 valance electrons which follow the orbital sequence as $1S^2$, $1P^6$, $1D^{10}$, $1F^6$, $2D^{10}$, $2S^2$, $1F^8$, $2P^6$, $1G^{12}$. Out of these 60 electrons, Ge_{12} cage contributes 48 valance electrons and remaining 12 electrons come from Au-transition metal atom. As per the prediction of Wade-Mingos rules [58–60], a close icosahedral transition metal-doped E_{12} cage structure can be formed for a system with $4n + 2 = 50$ valence electrons, in which 48 electrons are coming from the E_{12} cage cluster and the other two electrons are contributed from the net charge or from the subshell of transition metal atom. Following the explanation given by Goicoechea and McGrady [38], in the present case, out of 12 electrons of anionic Au atom, two electrons are contributing in the hybridization with the cage and remaining 10 electrons (in non-bonding orbitals) do not take part in hybridization. Therefore, the Ge_{12} cage contributes 48 valance electrons, 4 from each Ge atom with 2 electrons from cationic Au atom, fulfilling Wade-Mingos [58–60] rule. The assignment of the orbitals is shown in SI Fig. 2. Corresponding DOS and degeneracy in energy levels are shown in ESI Figs. 3 and 4.

Stability of anionic $AuGe_{14}$ cluster is straightforward. It is a cluster assembly which is composed of ground state $AuGe_7$ and the cage of Ge_7. Therefore, the hybridization takes place between Ge_7-Au^--Ge_7 units. As per the shell model, it has a shell closing number of valance electrons (68). Following the orbitals of the assembled cluster, we found both bonds and anti-bonds (see SI Fig. 2). It follows the sequence as $1S^2$ $1S^{*2}$ $1P^{*4}$ $1P^6$ $1P^{*2}$ $1D^6$ $1D^{*6}$ $2D^{10}$ $2S^2$ $2S^{*2}$ $1D^4$ $1D^{*4}$ $2P^4$ $2P^{*4}$ $1F^4$ $1F^{*4}1F^2$ (=68). Comparing the orbitals of anionic $AuGe_7$ and neutral Ge_7 orbitals, one can understand the assigned orbitals of anionic $AuGe_{14}$ cluster. Among these, in Au 2D, out of 10 electrons, 6 electrons are appearing as non-bonding electrons. Therefore, excluding the electrons present in anti-bonding, remaining 34 electrons are fulfilling the shell closing number. These electrons are $1S^2$ $1P^6$ $1D^6$ $2S^2$ $2D^4 1D^4$ $2P^4$ $1F^4 1F^2$. Similarly, orbital analysis of anionic $AuGe_{18}$ cluster gives the orbital sequence of 84 electrons as $1S^2$ $1S^{*2}$ $1P^2$ $1P^{*4}$ $1P^2$ $1P^{*2}$ $1P^2$ $1D^6$ $1D^{*2}$ $1D^2$ $1D^{*2}$ $1D^2$ $1D^{*6}$ $2D^{10}$ $2S^2$ $1F^2$ $2S^{*2}$ $1F^{10}$ $1F^{*4}$ $1F^2$ $1F^{*2}$ $1G^{14}$. Excluding the electrons associated in antibonding, total 58 electrons are taking part in bonding which is a shell-filled number. Here, hybridization takes place between three units: Ge_9-Au^--Ge_9. Here also, Au 2D orbitals are look localized, but they are not non-bonding orbitals. These electrons have a little role in hybridization. Except 1S, 1P, and 1D orbitals, all higher orbitals are not very close to the shape of the theoretical single-electron orbitals. Roles of Au 2D electrons are different from other clusters in this case, and this is clear from the DOS/PDOS figure. In the region, where 2D orbitals are appearing, at the position of each energy levels, one can find the considerable amount of contribution both from Au and Ge cages. Therefore, we cannot take it as non-bonding electrons. And it supports the role of 58 electrons in the cluster. Compare to the orbitals of cationic $AuGe_{18}$, the orbitals of $AuGe_{20}$ orbitals are clearer. The assigned orbitals are in the sequence: $1S^2$ $1S^{*2}$ $1P^2$ $1P^{*2}$ $1P^2$ $1P^{*2}$ $1P^2$ $1P^{*2}$ $1D^4$ $1D^{*2}$ $1D^2$ $1D^{*2}$ $1D^2$ $1D^{*4}$ $1D^2$ $2D^{10}$ $2S^2$ $1F^4$ $2S^{*2}$ $1F^6$ $1F^{*4}$ $1F^2$ $1F^{*2}$ $1F^2$ $1G^4$ $1F^{*4}$ $2P^2$ $1G^2$ $2P^4$ $2P^{*2}$ $1G^2$. As in the case of cationic $AuGe_{18}$, here also, Au orbitals are not non-bonding and they are taking part in the hybridization which is clear from the DOS. Therefore, shell model can be applied in all stable clusters as explained.

Stability and natural bond orbital

It is known that the hybridization between Ge and Au is of sp^3d type in general. Natural bond orbital (NBO) analysis can give a detail picture about the percentage hybridization in each

cluster from different levels of the constituent elements. In the present calculation, complete NBO analysis is shown in Fig. 5. In all stable clusters, except $n = 12$, there is a relative peak in the hybridization between Ge s, p, and Au d orbitals. The minima in anionic $AuGe_{12}$ is due to the role of Au p orbital which is not been counted in the graph. It is dominating among all Au p contribution in the clusters (see column plot).

The same is true for $n = 15$–17 and 19 sized clusters. The structural symmetry and aromaticity of $n = 12$ enhances its stability, which is not the same for $n = 15$–17 and 19 sized clusters. Therefore, though the sp^3d hybridization contribution in $n = 12$ clusters is less, but it is stable due the higher values of thermodynamic parameters. Whereas, for other stable clusters, both thermodynamic and kinetic parameters are consistent with the sp^3d hybridization. Therefore, complete NBO analysis supports the stability of $n = 7$, 10, 14, 18, and 20 clusters.

IR and Raman

In addition to the study of electronic structure and stabilities of these clusters, one of the key objectives of this work is to examine the vibrational properties of stable clusters (ESI Fig. 5) and where it can be used. In order to get vision into this work, we compare the IR and Raman results of different clusters with the variation of the variation of their size. Since the vibrational spectra are unique structural fingerprints of the clusters, therefore, easy structural identification is possible experimentally with the theoretical IR and Raman vibrational information. Both IR and Raman frequencies of the stable clusters are lying between the frequency range 50 to 300 cm except for $n = 20$ cluster. It has frequency range from very close to zero to 300 cm. The IR and Raman spectra shown in Fig. 6 have been generated based on the true IR and Raman frequencies with a Gaussian width close to 3 cm. This range falls within the far infrared region. FIR wavelength is too long to be apparent by the eyes; however, the animal body experiences its energy as a gentle radiant heat which can penetrate the skin up to 1.5 in. (in case of human body) produce any obvious skin heating can also have biological effects. This is effective for muscular damage repair and other related effect. In the present case, the IR and Raman spectra for $n = 7$, 10, 12, and 14 are very prominent and sharp. Only few dominating frequencies are present. However, for $n = 18$ and 20, a number of frequencies are present. This could be due to their structure linked with a single Au atom. Absence of any imaginary frequency means that all vibrational modes in the structures are acceptable without any resonance mode. Therefore, these stable structures could be useful to produce the FIR frequencies for different medical applications.

Conclusions

In the present theoretical study, thermodynamic and chemical stabilities of neutral $AuGe_n$ ($n = 1$–20) clusters have been performed in a systematic way using density functional theory. The structure prediction and global minima in each size are located using USPEX and VASP. Calculated results reveal a highly stable cationic $AuGe_7$ $AuGe_{10}$, $AuGe_{12}$ clusters, and $AuGe_{14}$, $AuGe_{18}$, and $AuGe_{20}$ assembled clusters. These species are having considerable large orbital energy gaps, high adiabatic detachment energies, large fragmentation, and binding energy and appearing as global ground state clusters. The following conclusions can be made on the basis of the calculated results.

According to the variation of thermodynamic parameters, it is found that cationic $AuGe_7$, $AuGe_{10}$, $AuGe_{12}$, $AuGe_{14}$, $AuGe_{18}$, and $AuGe_{20}$ are the most stable species. It found that the BE in doped clusters are always higher than the pure germanium clusters. Overall variation of the thermodynamic parameters shows local maxima at the sizes of the stable clusters. Rapid growth in BE in the doped clusters, for $n < 10$, reflects the thermodynamic instability of these clusters. Above $n > 10$ variation of average BE is less. This indicates the thermodynamic stability of the bigger-sized clusters. Local peaks in EE, FE, and stability

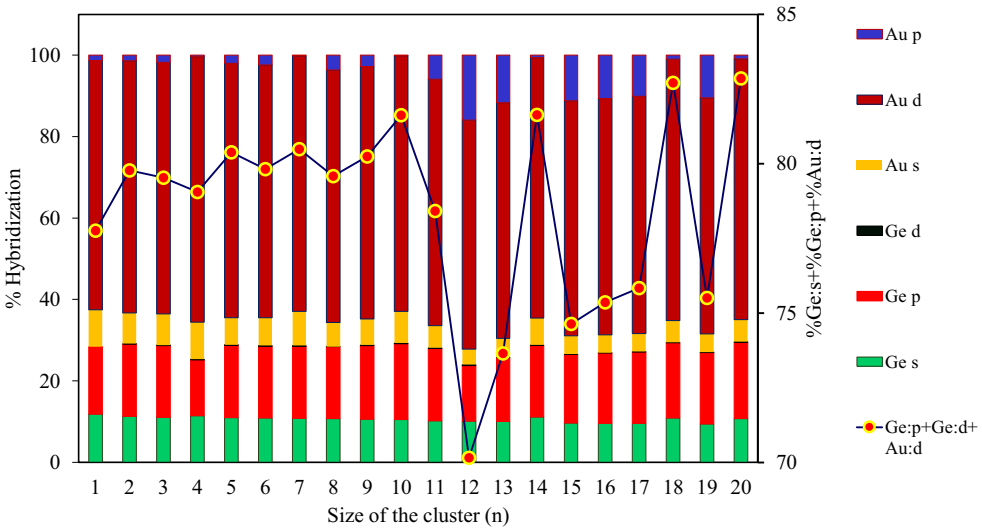

Fig. 6 Variation of % hybridization (Col. Plot: Av. Contribution/Ge atom + Au atom) and %Ge:s + %Ge:p + %Au:d with the cluster size

parameters support the BE variation of BE curve. One of the most important results of the present calculation is the variation of HOMO-LUMO gap and VIP. Both of these parameters are more or less similar to previously reported values [43,44]. The sharp drop in IP when a Ge atom is added at $n = 7$, 10, 12, 14, and 18 supports the shell-filled configuration of these clusters. This is precisely what can be seen in the AIP values of these clusters as shown in Fig. 4. Sharp drop in IP with the increase of the cluster size from n to $n + 1$ is possibly the strongest indication to support shell-filled cluster. Calculated AIP and VDE drops considerably when the cluster size increases from the sizes of the stable clusters $n = 7$, 10, 12, 14, and 18. These values are close to the experimentally as well as theoretically calculated AIP and VDE by Lu et al. [44]. Enhanced stabilities of these clusters have been explained by existing rules, such as shell-filled model, the mixed (π-σ) aromatic rule [57], and Wade-Mingos rules [58–60]. NBO analysis shows that except cationic $AuGe_{12}$ cluster, stability of the other cluster can be supported because of high sp^3d hybridization between germanium cage and gold atoms. Whereas, contribution of Au –p orbitals in cage clusters are considerable higher that the stable clusters with higher sp^3d hybridization. Calculated IR and Raman frequencies show that these frequencies fall in the far infrared region of electromagnetic radiation which could be useful for different medical purpose within a narrow region of the body.

Identification of the stable species and variation of chemical properties with size in the TM-doped Ge clusters will help us to design Ge-Au-based superatoms that can be future building blocks for cluster-assembled designer materials and could open up a new field in electronic industry. The present work could be the preliminary step in this direction and will be followed by more detailed studies on these systems in the near future.

Compliance with ethical standards

Conflict of interest The author declares that he has no conflict of interest.

Publisher's Note Springer Nature remains neutral with regard to jurisdictional claims in published maps and institutional affiliations.

References

1. Kumar V, Kawazoe Y (2001) Metal-encapsulated icosahedral superatoms of germanium and tin with large gaps: $ZnGe_{12}$ and $CdSn_{12}$. Appl Phys Lett 80:5
2. Zhang X, Wang Y, Wang H, Lim A, Gantefoer G, Bowen KH, Reveles JU, Khanna SN (2013) On the existence of designer magnetic Superatoms. J Am Chem Soc 135(12):4856
3. Reber AC, Khanna SN, Castleman Jr AW (2007) Superatom compounds, clusters, and assemblies: ultra-alkali motifs and architectures. J Am Chem Soc 129(33):10189
4. Bandyopadhyay D, Kaur P, Sen P (2010) New insights into applicability of Electron-counting rules in transition metal encapsulating Ge cage clusters. J Phys Chem A 114:12986
5. Kaxiras E, Jackson K (1993) Shape of small silicon clusters. Phys Rev Lett 71:727
6. Bandyopadhyay D, Sen P (2010) Density functional investigation of structure and stability of Ge_n and Ge_nNi (n= 1− 20) clusters: validity of the electron counting rule. J Phys Chem A 114:1835
7. Bandyopadhyay D (2008) A density functional theory–based study of the electronic structures and properties of cage like metal doped silicon clusters. J Appl Phys 104:084308
8. Bandyopadhyay D (2009) The study of the electronic structures and properties of pure and transition metal-doped silicon nanoclusters: a density functional theory approach. Mol Simul 35:381
9. Bandyopadhyay D (2012) Architectures, electronic structures, and stabilities of cu-doped gen clusters: density functional modeling. J Mol Model 18:737
10. Bandyopadhyay D (2009) Density functional study of the electronic structure and properties of lithium intercalated graphite. Eur Phys J D 54:643
11. Bandyopadhyay D, Kumar M (2008) The electronic structures and properties of transition metal-doped silicon nanoclusters: a density functional investigation. Chem Phys 353:170
12. Gopakumar G, Wang X, Lin L, Haeck JD, Lievens P, Nguyen MT (2009) Lithium-doped germanium nanowire? Experimental and theoretical indication. J Phys Chem C 113:10858
13. Gopakumar G, Lievens P, Nguyen MT (2007) Stability and thermodynamics of ligand-free germanium-gold clusters. J Phys Chem A 111:4353
14. Kamata Y (2008) High-k/Ge MOSFETs for future nanoelectronics. Mater Today 11:30–38
15. Pillarisetty R (2011) Academic and industry research progress in germanium nanodevices. Nature 479:324–328
16. Zhao W-J, Wang Y-X (2008) Geometries, stabilities, and electronic properties of FeGen (n = 9–16) clusters: Density-functional theory investigations. Chem Phys 352:291–296
17. Wang J, Han J-G (2006) A Theoretical Study on Growth Patterns of Ni-Doped Germanium Clusters. J Phys Chem B 110:7820–7826
18. Jing Q, Tian FY, Wang YX (2008) No quenching of magnetic moment for the Ge_nCo (n=1-13) clusters: first-principles calculations. J Chem Phys 128:124319
19. Wang J, Han J-G (2006) Geometries and electronic properties of the tungsten-doped germanium clusters: WGe_n (n = 1−17). J Phys Chem A (46):12670–12677
20. Zhao W-J, Wang Y-X (2009) Geometries, stabilities, and magnetic properties of $MnGe_n$ (n = 2–16) clusters: density-functional theory investigations. Theochem 901:18–23
21. Deng X-J, Kong X-Y, Xu X-L, Xu H-G, Zheng W-J (2014) Structural and bonding properties of small $TiGe_n^-$ (n = 2–6) clusters: photoelectron spectroscopy and density functional calculations. RSC Adv 4:25963–25968
22. Deng XJ, Kong XY, Xu XL, Xu HG, Zheng WJ (2014) Structural and magnetic properties of $CoGe_n^-$ (n=2–11) clusters: photoelectron spectroscopy and density functional calculations. Chem Phys Chem 15:3987–3993
23. Furuse S, Koyasu K, Atobe J, Nakajima A (2008) Experimental and theoretical characterization of MSi_{16}^-, MGe_{16}^-, MSn_{16}^- and MPb_{16}^- (M= Ti, Zr, and Hf): the role of cage aromaticity. J Chem Phys 129:064311
24. Deng X-J, Kong X-Y, Xu H-G, Xu X-L, Feng G, Zheng W-J (2015) Photoelectron spectroscopy and density functional calculations of VGe_n^- (n = 3–12) clusters. J Phys Chem C 119:11048–11055
25. Wang J, Han J-G (2007) The growth behaviors of the Zn-doped different sized germanium clusters: A density functional investigation. Chem Phys 342:253–259

26. Wang J, Han J-G (2008) Geometries, stabilities, and vibrational properties of bimetallic Mo_2-doped Ge_n (n = 9−15) clusters: a density functional investigation. J Phys Chem A 112:3224–3230
27. Beck SM (1987) Studies of silicon cluster–metal atom compound formation in a supersonic molecular beam. J Chem Phys 87:4233
28. Beck SM (1989) Mixed metal–silicon clusters formed by chemical reaction in a supersonic molecular beam: implications for reactions at the metal/silicon interface. J Chem Phys 90:6306
29. Wang J, Han JG (2007) The growth behaviors of the Zn-doped different sized germanium clusters: a density functional investigation. Chem Phys 342:253
30. Abreu MB, Reber AC, Khanna SN (2014) Does the 18-Electron rule apply to $CrSi_{12}$? J Phys Chem Lett 5:3492
31. Chauhan V, Abreu MB, Reber AC, Khanna SN (2015) Geometry controls the stability of $FeSi_{14}$. Phys Chem Chem Phys 17:15718–15724
32. Abreu MB, Reber AC, Khanna SN (2015) Making sense of the conflicting magic numbers in WSi_n clusters. J Chem Phys 143:074310
33. Dhaka K, Bandyopadhyay D (2015) Study of the electronic structure, stability and magnetic quenching of $CrGe_n$ (n=1–17) clusters: a density functional investigation. RSC Adv 5:83004–83012
34. Reveles JU, Khanna SN (2005) Nearly-free-electron gas in a silicon cage. Phys Rev B 72:16513
35. Koyasu K, Akutsu M, Mitsui M, Nakajima A (2005) Selective formation of MSi_{16} (M = Sc, Ti, and V). J Am Chem Soc 127:4998
36. Berlicki TM, Murawski E, Muszynski M, Osadnik SJ, Prociow EL (1995) Thin-film thermocouples of Ge doped with au and B. Sens Actuators, A 50:183–186
37. Wang XX, Getaneh M, Martoff CJ, Kaczanowicz E (1999) Hot electron effects and dynamic behavior of gold doped germanium thin films as cryogenic phonon sensors. J Appl Phys 85:8274–8280
38. Goicoechea JM, McGrady JE (2015) On the structural landscape in endohedral silicon and germanium clusters, $M@Si_{12}$ and $M@Ge_{12}$. Dalton Trans 44:6755–6766
39. McDermott D, Newman KE (2015) Wade's rules and the stability of Au_nGe_m clusters. Eur Phys J D 69:90–102
40. Li X, Su K, Yang X, Song L, Yang L (2013) Effect of alkali metal atoms doping on structural and nonlinear optical properties of the gold-germanium bimetallic clusters. J Comput Chem 1010:32–37
41. Truong BT, Nguyen MT (2011) Enhanced stability by three-dimensional aromaticity of Endohedrally doped clusters $X_{10}M^{0/-}$ with X = Ge, Sn, Pb and M = cu, ag, au. J Phys Chem A 115:9993–9999
42. Li X-J, Ren H-J, Yang L-M (2012). J Nanomater 2012:1–8
43. Mahtout S, Siouani C, Rabilloud F (2018) Growth behavior and electronic structure of Noble metal-doped germanium clusters. J Phys Chem A 122:662–677
44. Lu S-J, Hu L-R, Xu X-L, Xu H-G, Chen H, Zheng W-J (2016) Transition from exohedral to endohedral structures of $AuGe_n$ (n = 2–12) clusters: photoelectron spectroscopy and ab initio calculations. Phys Chem Chem Phys 18:20321
45. Perdew JP, Burke K, Ernzerhof M (1996) Generalized gradient approximation made simple. Phys Rev Lett 77(18):3865–3868
46. Perdew JP, Burke K, Ernzerhof M (1997) Generalized gradient approximation made simple [ERRATA: Phys. Rev. Lett. 77, 3865 (1996)]. Phys Rev Lett 78(7):1396
47. Frisch MJ, Trucks GW, Schlegel HB, Scuseria GE, Robb MA, Cheeseman JR, Scalmani G, Barone V, Mennucci B, Petersson GA, Nakatsuji H, Caricato M, Li X, Hratchian HP, Izmaylov AF, Bloino J, Zheng G, Sonnenberg JL, Hada M, Ehara M, Toyota K, Fukuda R, Hasegawa J, Ishida M, Nakajima T, Honda Y, Kitao O, Nakai H, Vreven T, Montgomery Jr JA, Peralta JE, Ogliaro F, Bearpark M, Heyd JJ, Brothers E, Kudin KN, Staroverov VN, Kobayashi R, Normand J, Raghavachari K, Rendell A, Burant JC, Iyengar SS, Tomasi J, Cossi M, Rega N, Millam JM, Klene M, Knox JE, Cross JB, Bakken V, Adamo C, Jaramillo J, Gomperts R, Stratmann RE, Yazyev O, Austin AJ, Cammi R, Pomelli C, Ochterski JW, Martin RL, Morokuma K, Zakrzewski VG, Voth GA, Salvador P, Dannenberg JJ, Dapprich S, Daniels AD, Farkas O, Foresman JB, Ortiz JV, Cioslowski J, Fox DJ (2009) Gaussian 09, Revision A.1. Gaussian, Inc., Wallingford CT
48. Dolg M, Wedig U, Stoll H, Pereuss H (1987) Energy-adjusted ab initio pseudopotentials for the first row transition elements. J Chem Phys 86:866
49. Glass CW, Oganov AR, Hansen N (2006) USPEX – evolutionary crystal structure prediction. Comput Phys Commun 175:713
50. Kresse G, Furthmüller J (1996) Efficient iterative schemes for *ab initio* total-energy calculations using a plane-wave basis set. Phys Rev B 54:11169
51. Kresse G, Joubert D (1999) From ultrasoft pseudopotentials to the projector augmented-wave method. Phys Rev B 59:1758
52. Bandyopadhyay D (2009) Study of pure and doped hydrogenated germanium cages: a density functional investigation. Nonotechnology 20:275202
53. Kumar M, Singh BJ, Kajjam S, Bandyopadhyay D (2010) Effect of transition metal doping on hydrogenated germanium Nano-cages: a density functional investigation. J Comp Theo Nanoscience 7(1):296
54. Trivedi R, Dhaka K, Bandyopadhyay D (2014) Study of electronic properties, stabilities and magnetic quenching of molybdenum-doped germanium clusters: a density functional investigation. RSC Adv 4:64825–64834
55. Yoshida S, Fuke K (1999) Photoionization studies of germanium and tin clusters in the energy region of 5.0–8.8 eV: ionization potentials for Ge_n (n=2–57) and Sn_n (n=2–41). J Chem Phys 111:3880
56. Zhou B, Kramer T, Thompson AL, McGrady JE, Goicoechea JM (2011) A highly distorted open-Shell endohedral Zintl cluster: $[Mn@Pb_{12}]^{3-}$. Inorg Chem 50:8028
57. Tai TB, Nguyen HMT, Nguyen MT (2011) The group 14 cationic clusters by encapsulation of coinage metals X10M+, with X = Ge, Sn, Pb and M = cu, ag, au: enhanced stability of 40 valence electron systems. Chem Phys Lett 502:187
58. Wade K (1971) The structural significance of the number of skeletal bonding electron-pairs in carboranes, the higher boranes and borane anions, and various transition-metal carbonyl cluster compounds. J Chem Soc D:792
59. Wade K (1976) Structural and Bonding Patterns in Cluster Chemistry. Adv Inorg Chem Radiochem 18:1
60. Mingos DMP (1972) A general theory for cluster and ring compounds of the Main group and transition elements. Nat Phys Sci 236:99
61. Huang X, Xu H-G, Lu S, Su Y, King RB, Zhao J, Zheng W (2014) Discovery of a silicon-based ferrimagnetic wheel structure in $VxSi_{12}^-$ (x = 1–3) clusters: photoelectron spectroscopy and density functional theory investigation. Nanoscale 6:14617
62. Esenturk EN, Fettinger J, Eichhorn B (2006) The Pb_{12}^{2-} and Pb_{10}^{2-} Zintl Ions and the $M@Pb_{12}^{2-}$ and $M@Pb_{10}^{2-}$ Cluster Series Where M = Ni, Pd, Pt. J Am Chem Soc 128:9178
63. Uta MM, Cioloboc D, King RB (2012) Cobalt-centered ten-vertex germanium clusters: the pentagonal prism as an alternative to polyhedra predicted by the Wade-Mingos rules. Inorg Chem 51:3498–3504
64. Hirsch A, Chen Z, Jiao H (2000) Spherical aromaticity in I_h symmetrical fullerenes: the $2(N+1)^2$ rule. Angew Chem Int Ed 39:3915